ACI MATERIALS JOURNAL TECHNICAL PAPER

Title no. 87-M2

Antiplane Shear Fracture Tests (Mode III)

By Zdeněk P. Bažant, Pere C. Prat, and Mazen R. Tabbara

Mode III (antiplane) shear-fracture energies of concrete and mortar were measured on the basis of the size-effect law. The specimens were cylinders with a circumferential notch at their midlengths, subjected to pure torsion at zero axial force. The specimens were geometrically similar and their sizes varied as 1:2:4. The mortar specimens were observed to behave in a manner closer to linear elastic fracture mechanics than did the concrete specimens. The ratio of Mode III to Mode I (tensile) fracture energies was found to be about 3 for concrete and about 8 for mortar. The results indirectly indicate that a volume expansion of the sheared fracture-process zone may be a significant mechanism causing transverse tensile stresses across the ligament. The size-effect measurements also yield an estimate of the size of the fracture-process zone, which is found to be nearly the same as for Mode I fracture.

Keywords: concretes; cracking (fracturing); dimensional analysis; energy; measurement; mortars (material); shear tests; specimens; tensile stresses; tests.

Until recently it had been generally accepted that fracture in concrete is always tensile and propagates in the direction normal to the maximum principal stress. Such behavior is indeed observed in the diagonal shear failure and torsional failure of beams, as well as in punching-shear failure of slabs. The existence of shear fracture in brittle materials has been denied, and even such claims as "shear fracture is sheer nonsense" have been heard.

Doubts arose, however, when dynamic tests of certain concrete box structures loaded by short pressure pulses caused the top slabs to fail by direct shear next to the supports. As a result of this and other experiences, tests of shear fracture were undertaken at Northwestern University[1] using edge-notched specimens of Iosipescu geometry loaded in Mode II (in-plane shear). The size-effect method was used in those tests to determine the Mode II fracture energy. Interpretation of those tests was not unambiguous, because a perfectly antisymmetric Mode II field at the crack tips is not achieved in this type of test, not only in the actual nonlinear behavior, but also according to the theory of elasticity. The elastic solution of the stress field near the crack tips in those specimens indicates the presence of compressive stresses across the crack-line extension, which represents deviations from the ideal Mode II conditions. In theory, a perfect Mode II shear loading could be achieved in an elastic specimen of that type, but this would require applying additional antisymmetric tensile forces, as shown in Reference 1, which would be difficult to carry out. Moreover, as pointed out by Ingraffea and Panthaki[2] in a dialogue with Bažant and Pfeiffer,[3] the failure of these specimens might be partly caused by axial compression splitting (similar to the Brazilian split-cylinder test), which again prevents attaining pure Mode II shear conditions.

To gain additional insight, Bažant and Prat[4] decided to study Mode III (antiplane shear) rather than Mode II (in-plane shear). Using cylindrical specimens with a circumferential notch subjected to torsion (Fig. 1 and 2), they carried out Mode III fracture tests of concrete, which apparently had not been conducted previously. According to the theory of elasticity, the applied torque produces a stress and deformation field that is perfectly antisymmetric with regard to the crack plane; thus, a planar crack represents a pure shear crack. The size-effect method[5-8] has been used to determine the Mode III fracture energy of concrete G_f^{III}. Surprisingly, the value of G_f^{III} obtained from these tests has been much smaller than the value of the Mode II fracture energy G_f^{II} obtained from the preceding tests of notched beams, although still larger than the Mode I (opening mode) fracture energy G_f^{I}. It apperared that the value of shear-fracture energy might not represent a material constant but could be a function of the normal stress across the crack plane, and that the value of this stress might in turn depend on the volume changes in the fracture process zone. This conclusion was supported by the finding that torsional loading in a triaxial torsional testing machine that produces axial confinement and prevents free axial expansion of the cylinder leads

ACI Materials Journal, V. 87, No. 1, January-February 1990.
Received Aug. 18, 1988, and reivewed under Institute publication policies.
 Pertinent discussion will be published in the November-December 1990 *ACI Materials Journal* if received by Aug. 1, 1990.

Zdeněk P. Bažant, FACI, is a professor at Northwestern University, Evanston, Ill., where he recently served as Director of the Center for Concrete and Geomaterials. Dr. Bažant is a registered structural engineer, a consultant to Argonne National Laboratory, and is on the editorial boards of several journals. He is Chairman of ACI Committee 446, Fracture Mechanics; a member of ACI Committees 209, Creep and Shrinkage in Concrete; and 348, Structural Safety; and Chairman of RILEM's committee on creep and SMiRT's Division H. In 1987, Professor Bažant visited the University of Tokyo as Kajima Foundation Fellow and has been NATO senior guest scientist at E.N.S., Paris-Cachan.

ACI member Pere C. Prat is a scientific research associate at the Materials Science Institute (CSIC), Barcelona, Spain. He obtained his civil engineering degree from the School of Civil Engineering of the Technical University of Catalonia, Barcelona, Spain, in 1982, and his PhD from Northwestern University in 1987. His research interests include constitutive models for geomaterials, strain-softening behavior, fracture mechanics, nonlinear analysis of concrete structures, experimental methods, and finite element applications.

ACI member Mazen R. Tabbara is a graduate research assistant at Northwestern University, Evanston, Illinois. His research interests include constitutive models for concrete, fracture mechanics, and finite element applications.

to a nonplanar failure mode; see the conical failure surfaces in Fig. 3.

The purpose of this paper is to examine these questions more deeply, report the results of a larger series of Mode III failure tests that included mortar specimens as well as concrete specimens, determine the Mode III fracture energy, and examine the applicability of the size-effect law. An additional purpose is to extract from the test results an estimate for the length of the fracture process zone. The significance of this research is expected to be an improved ability to predict brittle failures of concrete structures.

The torsional fracture specimen conceived by Bažant and Prat[4] was independently also introduced by Suresh and Tschegg[9] to study mixed-mode fracture of fatigued ceramics. Using combined torsional-axial loading, Suresh and Tschegg determined a failure surface in terms of the Mode III and Mode I stress-intensity factors. Their conclusions on the effect of axial stresses are similar to those made by Bažant and Prat and are extended further here.

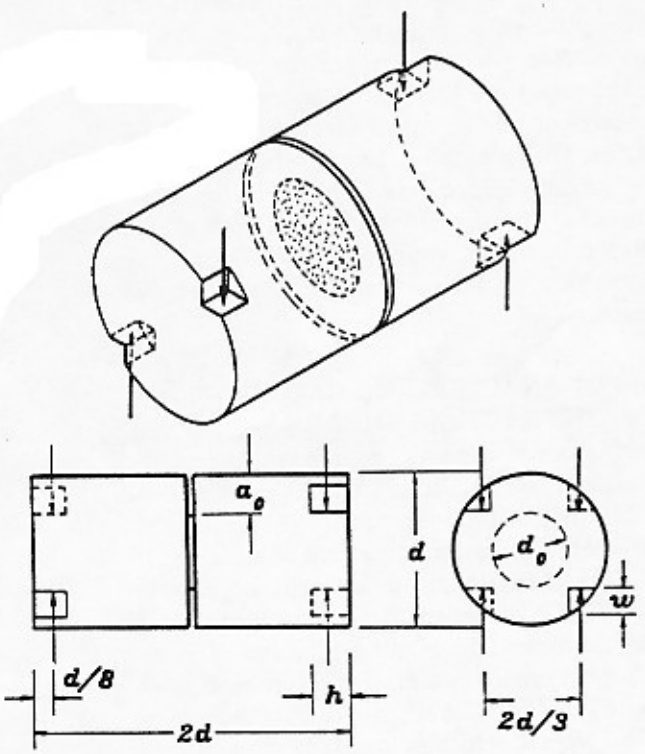

Fig. 1 — Torsional circumferentially notched fracture specimens

EXPERIMENTAL INVESTIGATION

To determine fracture energy by the size-effect method, geometrically similar specimens of significantly different sizes needed to be tested. Similar circumferentially notched cylinders of diameters d = 1.5, 3, and 6 in. (38, 76, and 152 mm) were used. The length-to-diameter ratio was ℓ/d = 2. Circular notches of thickness 1/16 in. (1.6 mm), located in the middle plane perpendicular to the axis of the cylinders (Fig. 1 and 2), were created by casting. The notch depth was a_0 = $d/4$.

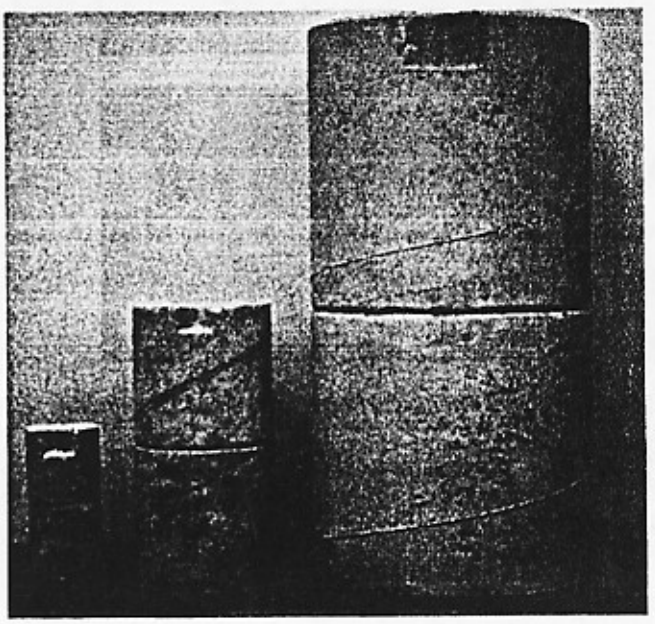

Fig. 2 — Geometrically similar notched specimens used in tests

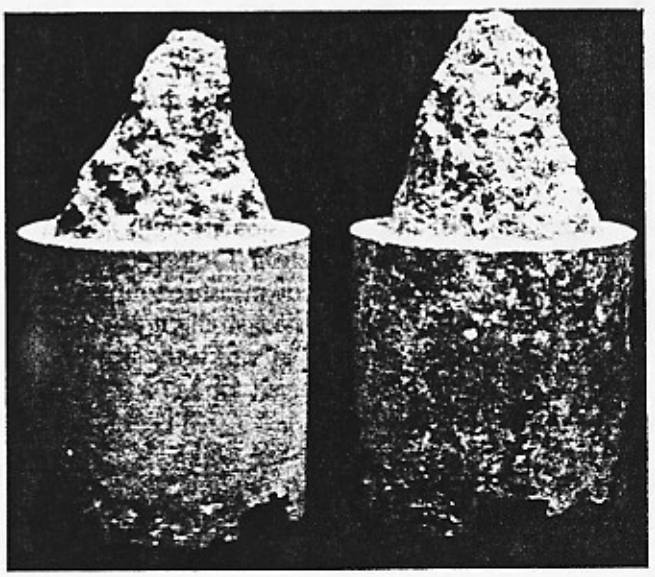

Fig. 3 — Conical failure surface observed in previous tests with restrained axial displacement

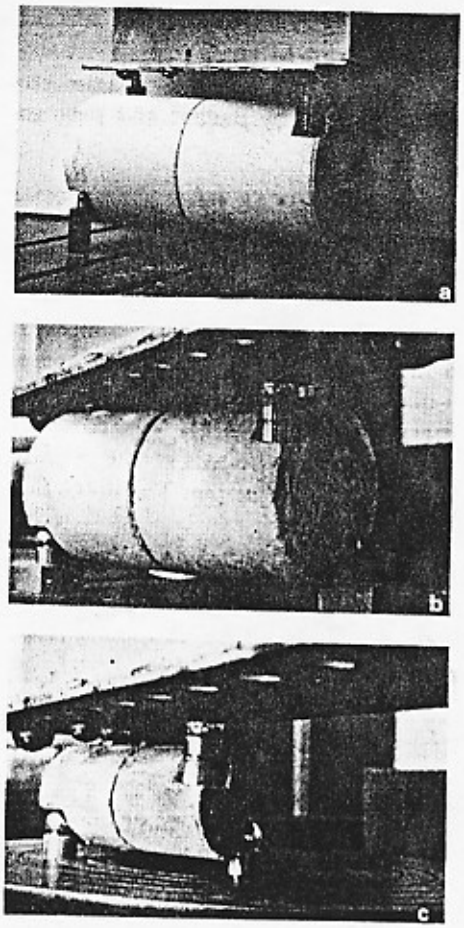

Fig. 4 — Specimens during testing in MTS machine

The torque T was applied at each end of the specimen as a couple, as shown in Fig. 1 and 4. The wedge-shaped cutouts on which the loads were applied were cast in a standard cylinder mold in which wooden inserts were placed. Each end-couple had an arm of $2d/3$ and was applied in a plane perpendicular to the axis of the specimen at a distance of $d/8$ from the ends.

Two test series were carried out, one for concrete and one for mortar. Each test series consisted of nine torsional specimens, three for each size (Fig. 2), plus three companion cylinders 3 in. (76 mm) in diameter and 6 in. (152 mm) long, to test for compression strength. All the specimens and control cylinders for each test series were cast from the same batch. The means and standard deviations of the compression strength f'_c after 28 days of moist curing are given in Table 1. The 28-day f'_c values for concrete were not measured directly, but calculated from the compression strength $f'_c(35)$, measured at the time of the tests at which the age of concrete was 35 days. The adjustment for age was based on the approximate formula[10] $f'_c(t) = f'_c(28)\ [1 + 0.277 \log (t/28)]$ from which $f'_c(28) \simeq 0.974\, f'_c(35)$.

All specimens were cast with the longitudinal axis in a vertical position, to insure statistical homogeneity and isotropy within the notch plane. The concrete mix had a water-cement ratio of 0.6, and a cement-sand-gravel ratio of 1:2:2 (all ratios by weight). The concrete had maximum gravel size d_a = 0.5 in. (12.7 mm) and maximum sand-grain size of 0.19 in. (4.8 mm). The aggregate consisted of crushed limestone and siliceous Lake Michigan beach sand from Illinois. ASTM C 150 Type I portland cement, with no admixtures and no air-entraining agents, was used. The mortar mix had a water-cement ratio of 0.5 and a cement-sand ratio of 1:2. The same sand as for the concrete specimens was used, i.e., the maximum aggregate size was d_a = 0.19 in. (5 mm). The aggregate composition was thus the same as for the concrete specimens except for the omission of gravel. The water-cement ratio differed from that of the concrete specimens in order to achieve approximately the same workability.

Table 1 — Compression strength f'_c, psi

Mix	Mean	Standard deviation
Concrete	5633	221
Mortar	5365	624

The specimens were cast in waxed cardboard molds from which they were removed after one day. Subsequently, they were cured in a moist room at 95 percent humidity and 80 F temperature until about 1 hr before the test. The tests of mortar specimens were made at the age of 28 days. The age of the concrete specimens at the time of test was 35 days, instead of the standard 28 days, because of a delay due to the repair of equipment. Fig. 4 shows the specimens of all sizes installed in the testing machine. The values of the strength and fracture energy for the age of 28 days were obtained by adjusting the 35-day values.

Fig. 5 exhibits the fractured concrete specimens after testing and demonstrates that the fracture surface was planar and did not propagate in the direction normal to the maximum principal stress, which is inclined. A similar fracture surface was observed for the mortar specimens. All the tests were carried out at room temperature in a closed-loop MTS machine under stroke-control conditions. The loading rates were chosen such that the time to maximum load was 3 to 5 min for specimens of all sizes. The size-effect method, used to calculate the fracture energy, required knowledge of only the maximum load, from which the maximum torque was then calculated.

SIZE-EFFECT ANALYSIS AND CALCULATION OF FRACTURE ENERGY

Size effect is understood as the dependence of the nominal stress at maximum load (failure) τ_N on a characteristic dimension of the specimen d, when geometrically similar specimens or structures are considered. In the case of three-dimensional similarity, τ_N is generally defined as $\tau_N = CP/d^2$, where P = maximum load, d = characteristic dimension of the body, and C = arbitrary nondimensional constant. For the present specimens $\tau_N = 16T/\pi d^3 = CP/d^2$, where T = maximum torque; $C = 16R/\pi d$, which is constant since R/d = constant for geometrically similar specimens; and $T = PR$ where R is the arm of the force couple applied at the ends. Note that the value of C has no effect on the

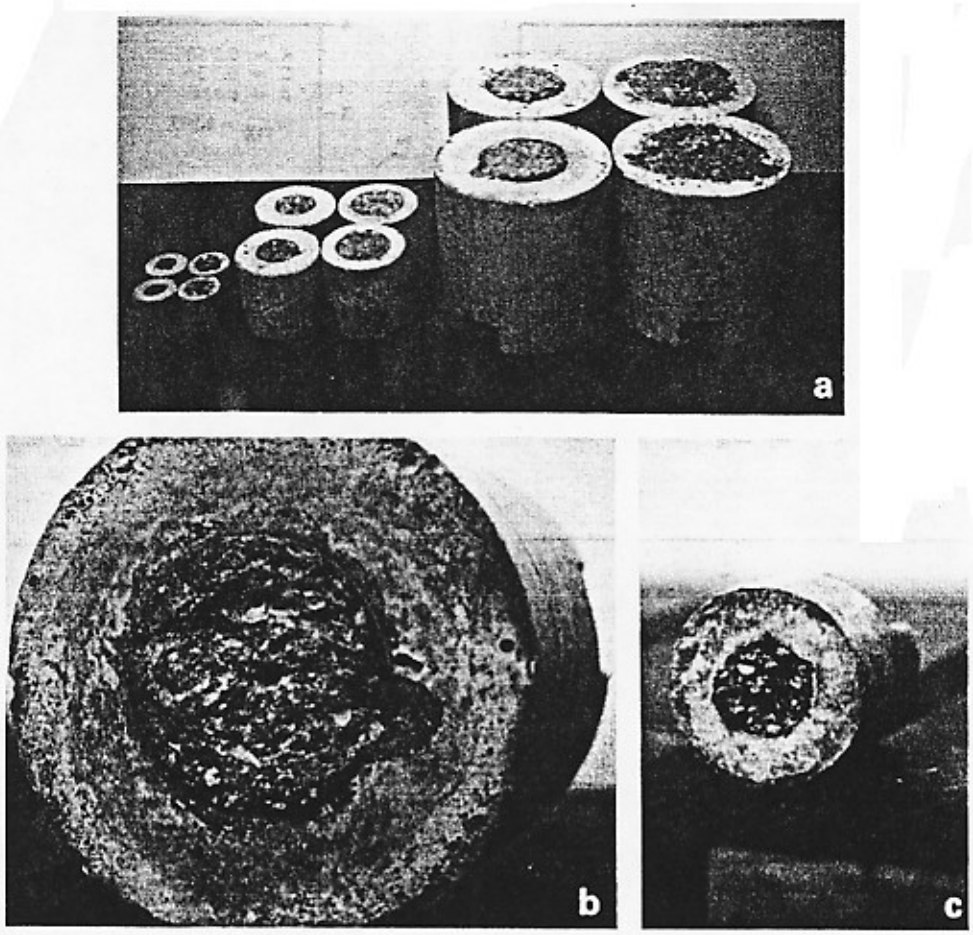

Fig. 5 — Fractured specimens after testing, showing the failure surfaces

values of fracture energy given by Eq. (3), which follows. The value of τ_N as defined represents the maximum elastic stress if there were no notch or crack.

Because the cracks in concrete propagate with a relatively large microcracking zone which blunts the fracture front, the size effect represents a transition between the plastic limit analysis for which there is no size effect (i.e., τ_N is constant), and the classical linear-elastic fracture mechanics for which the size effect is the strongest possible and which is of the type $\tau_N \sim d^{-1/2}$. The transition may be described by the approximate size-effect law[5]

$$\tau_N = Bf_t' \left(1 + \frac{d}{\lambda_0 d_a}\right)^{-1/2} \qquad (1)$$

where B and λ_0 are empirical constants, d_a is the maximum size of aggregate, and f_t' is the tensile strength of concrete. Eq. (1) has been derived in References 5 and 11, and for three dimensions in Reference 12. It has been experimentally validated in Mode I (opening) fracture[6] and was also found to approximately apply to the quasi-Mode II (shear) fracture tests in Reference 1, and to diagonal shear.[13] Tests showed that Eq. (1) is also applicable to various brittle failures of concrete structures, such as failure of beams in torsion, punching-shear failure of slabs, failure of pipes, etc.[14-16]

To determine parameters B and λ_0, Eq. (1) may be transformed to the form

$$\left(\frac{f_t'}{\tau_N}\right)^2 = \frac{1}{B^2 \lambda_0}\left(\frac{d}{d_a}\right) + \frac{1}{B^2} \qquad (2)$$

Eq. (2) represents a linear relation between $(f_t'/\tau_N)^2$ and d/d_a, and may be rewritten as $Y = AX + C$, where $Y = (f_t'/\tau_N)^2$, $X = d/d_a$, $C = 1/B^2$, and $A = C/\lambda_0$. A linear regression of the test results may be used to determine A and C, from which $B = C^{-1/2}$ and $\lambda_0 = C/A$. The regression analysis also yields the statistics of the errors. Fig. 6 and 7 give the coefficient of variation $\omega_{Y|X}$ of the vertical deviations from the regression line and the correlation coefficient ρ.

As proposed in References 11 and 12, the concrete fracture energy G_f may be uniquely defined as the energy release rate required for crack propagation in an infinitely large specimen. In theory, this definition must yield results that are independent of both the size and the shape of the specimen, provided that the correct size-effect law is known. The exact size-effect law is unknown, but the approximate size-effect law in Eq. (1) has been shown to be adequate for practical purposes, and valid for the size range 1:20 regardless of specimen shape. The following formula has been derived[7,11,12]

$$G_f = \frac{g(\alpha_0)}{AE_c} f_t'^2 d_a \qquad (3)$$

in which $\alpha_0 = a_0/r$; a_0 = notch depth; r = radius of the

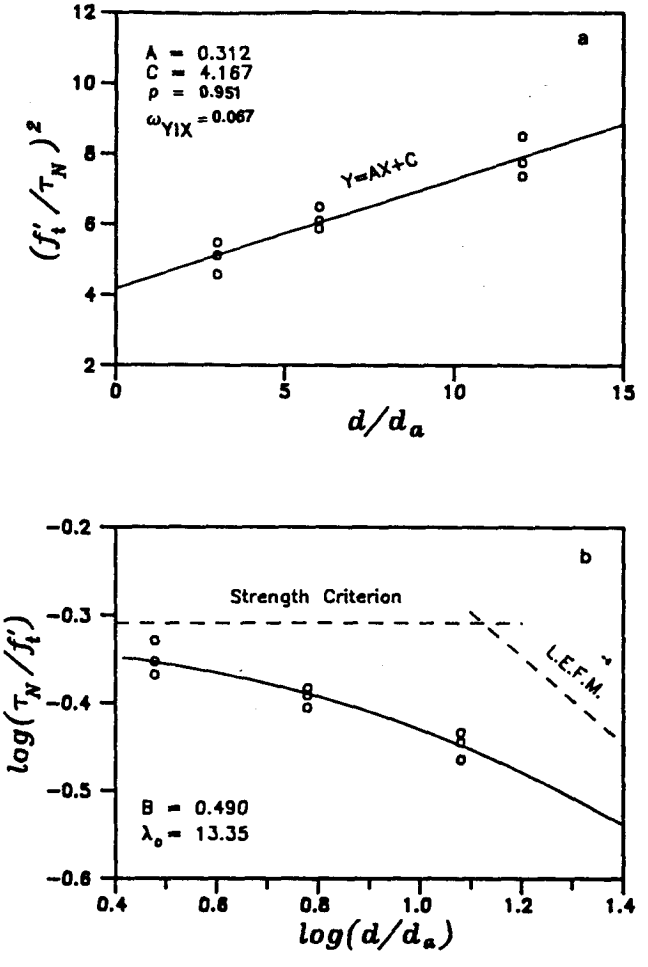

Fig. 6 — Results from tests of concrete specimens: (a) linear regression, and (b) size effect

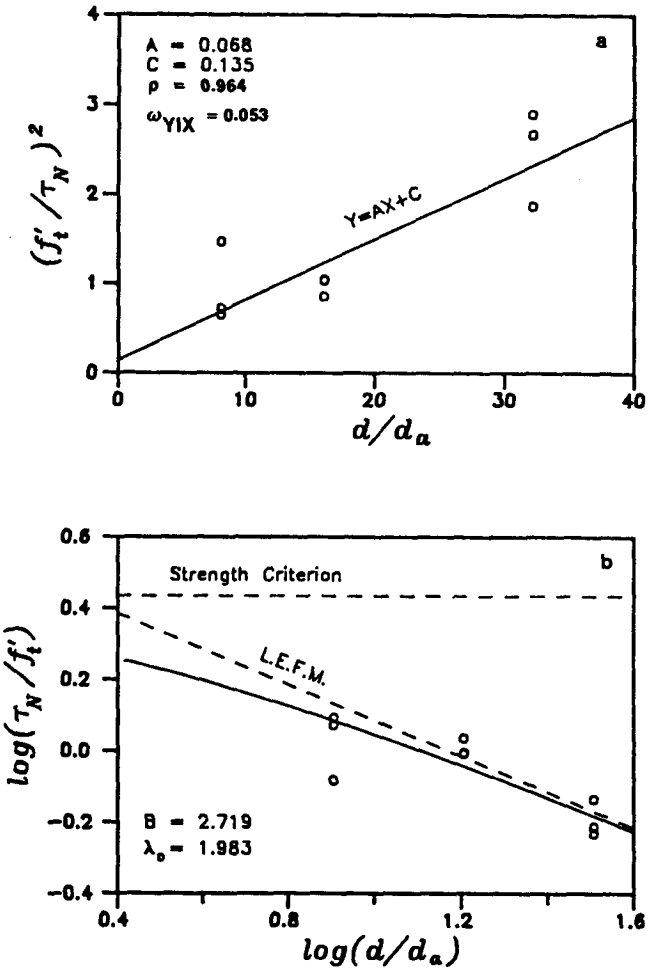

Fig. 7 — Results from tests of mortar specimens: (a) linear regression, and (b) size effect

Table 2 — Fracture energy G_f, lb/in. (N/m)

Mix	Mode I	Mode II	Mode III
Concrete	0.22 (39)	6.30 (1104)	0.61 (107)
Mortar	0.13 (23)	3.34 (585)	1.01 (177)

cylinder; E_c = modulus of elasticity of concrete; f_t' = direct tensile strength of concrete; $A = 1/(B^2\lambda_0)$ = slope of the regression line as already defined; $g(\alpha_0)$ = nondimensional energy release rate of the specimen according to the linear elastic fracture mechanics, which can be found for the basic specimen geometries in textbooks and handbooks,[17,18] and can in general be determined by linear finite element analysis. For the notch depth of $d/4$(i.e., $\alpha_0 = 0.5$), $\alpha\ (a_0) = 6.99\ (1 + \upsilon)$ where υ = Poisson's ratio. In the calculations it was assumed that $\upsilon = 0.18$.

The tensile strength was not measured but was estimated from the formula $f_t' \approx 6\sqrt{f_c'}$, where f_c' and f_t' are in psi (6895 Pa) and f_c' = standard cylindrical compression strength. Since the slope A of the linear regression plots is proportional to $f_t'^2$, an error in f_t' has no effect on the fracture-energy values.

The measured maximum torques are plotted in Fig. 6 and 7. The plots at the bottom demonstrate that the measured τ_N agrees with the size-effect law (solid curve). The plots at the top show the regression line, which yields the mean values of the parameters of the size-effect law.

The fracture-energy values obtained for concrete in this manner pertain to the age of 35 days. They were then transformed to 28 days, by using Bažant and Oh's empirical formula[19] $G_f = (2.72 + 0.0214\, f_t')\, f_t'^2\, d_a/E_c$, which yields $G_f(28) = 0.976G_f(35)$. The plots in Fig. 6 and 7 correspond to the 28-day values.

The values obtained for fracture energy are given in Table 2. For comparison, Table 2 also indicates the values for Modes I and II previously obtained from tests of essentially the same concrete and mortar.

Aside from the fracture energy, the size-effect law makes it possible to estimate the effective length c_f of the fracture process zone, using the formula[8]

$$c_f = \frac{d_0 g(\alpha_0)}{g'(\alpha_0)} \tag{4}$$

in which $g'(\alpha_0) = dg(\alpha)/d\alpha$ at $\alpha = \alpha_0$. The value of c_f represents the effective length of the fracture process zone for an infinitely large specimen, which is a material constant. The present test results yield the values

given in Table 3. For comparison, this table also shows the c_f values obtained from the previous test results[8] for Mode I. Notice the good agreement between Mode I and Mode III results, which suggests that c_f should indeed be a material property. Theoretically, the obtained value of c_f applies to an infinitely large specimen, but because Bažant's law is not sufficiently accurate for an inifinite size range, the value obtained for c_f applies to a size about ten times larger than that of the largest specimen tested.

ANALYSIS OF RESULTS

According to the size-effect law, the test results for mortar should be closer to linear elastic fracture mechanics than those for concrete, for the same specimens. This is confirmed by the present results; see Fig. 6 and 7 where the data points for mortar lie closer to the straight line asymptote of linear elastic fracture mechanics, whose slope is -0.5.

Comparison with the Mode II and Mode I fracture energies (Table 2) reveals a surprise. The values of G_f^{III} might have been expected to be about the same as G_f^{II}, and much larger than G_f^{I}. But this has not turned out to be the case; rather, the measured G_f^{III} is much smaller than G_f^{II}, but larger than G_f^{I}. The mechanism to explain this finding will require deeper study, but we shall attempt an approximate analysis.

A clue to the source of this discrepancy is provided by the experimetal observation that the results of shear fracture tests are very sensitive to the restraint of the specimen in the direction normal to the fracture plane (the axial direction of the cylinder for the present tests). In pilot tests, it was observed that very different results can be obtained if friction at the supports is not eliminated. The confinement of the shear fracture zone due to an axial friction force produced at the supports can no doubt raise the value of G_f significantly.

For the sake of comparison, another series of torsional tests of Mode III fracture was carried out with different equipment—a large triaxial torsional testing machine, which was very stiff because its 8.51 in. diameter test chamber is designed to resist chamber pressures up to 20,000 psi (138 MPa) plus axial forces up to 1,100,000 lb (4.89 mN). It was not surprising that the tests in this machine, which were made at essentially zero axial displacement at the ends of the cylindrical specimen, showed a different mode of failure, in which the failure surface was conical rather than planar (see Fig. 3). The axial restraint engenders an axial compressive force, which is known to be capable of altering the failure mode. The failure with a conical surface is nevertheless still of a shear type.

To explain the foregoing observations, it is logical to assume that G_f^{III} as well as G_f^{II} is not a material constant, but rather a material function $\phi(N_f)$ of the normal force N_f across the fracture process zone of length c_f, normal to the shear fracture plane (N_f is a force per unit length of the crack-front edge and has the dimension N/m). The function ϕ (N_f) should be the same for Mode II and Mode III shear fractures. For the same N_f,

Table 3 — Effective fracture process-zone length c_f, in. (mm)

Mix	Mode I	Mode III
Concrete	0.60 (15)	0.66 (17)
Mortar	0.06 (1.4)	0.04 (1.0)

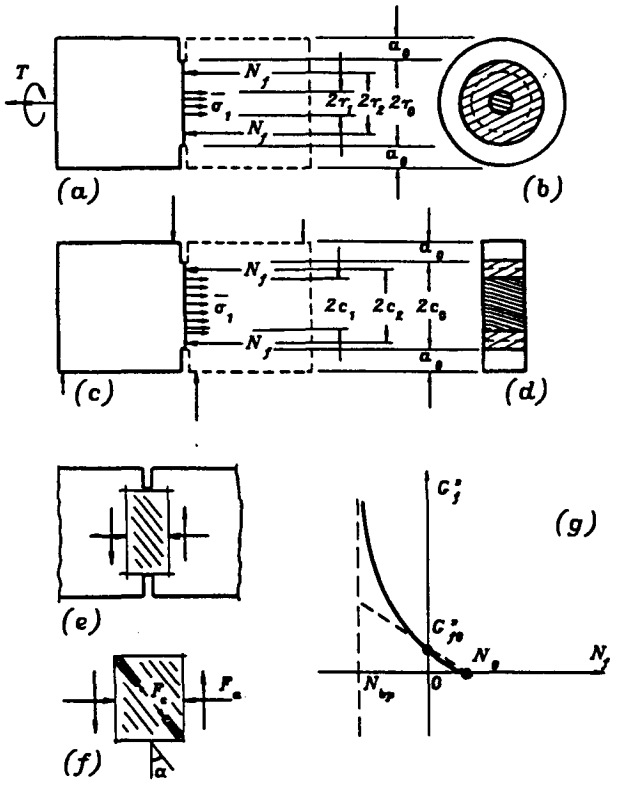

Fig. 8 — Transverse stresses and inclined microcracking induced in the fracture-process zone in shear-fracture tests

we should have $G_f^{II} = G_f^{III} = G_f^{*}$ = shear fracture energy (regardless of the mode) such that

$$G_f^{*} = \phi(N_f) \tag{5}$$

That G_f^{II} must in general strongly depend on N_f has already been corroborated in previous work[1] by finite element analysis of Mode II fracture tests. In fact, that study made the even more general assumption that both Mode I and II fractures can be modeled by the same stress-strain relation for the fracture process zone. The reason for different effective values of the fracture energy in Modes I and II can be found in the fact that, in shear, the microcracks in the fracture process zone are not parallel to the fracture plane, but are inclined to it by angle α [see Fig. 8(e) and (f)]. The column of intact material between adjacent inclined cracks carries compression force F_c. This force has an axial component F_a which must be resisted together by the tensile stresses in the undamaged portions of the ligament [σ_1 in Fig. 8(a)] and by the axial force provided by the support. If axial displacements are prevented, the inclined compressive forces F_c are high and can offer a large resistance to shear. Hence, the apparent values of frac-

ture energy must be large. If the axial displacements are free, the inclined compression forces must vanish and thus cannot contribute to transmit shear stresses across the fracture process zone, and then the apparent value of shear fracture energy is small.

The action just described was exhibited by a finite element model with a tensile softening stress-strain relation for the fracture process zone. Using such a model, Bažant and Pfeiffer[1] showed that the results of both Mode I and Mode II fracture tests can be matched with the finite element program using the *same* material properties. In this finite element analysis, one does not directly use the fracture energy. Rather, one uses a triaxial stress-strain relation such that the area under the implied uniaxial tensile stress-strain diagram equals G_f/w_c, where w_c = effective width of the fracture process zone.

As a crude approximate description of the role of the confining force N_f, we may write the longitudinal equilibrium condition assuming a zero axial resultant in the cross section. With the notation $\bar{\sigma}_1$= average tensile stress in the tensile zone of the ligament and r_1 = radius of this zone, and the equilibrium condition is $\pi r_1^2 \bar{\sigma}_1 = -2\pi r_2 N_f$ or $N_f = -\bar{\sigma}_1 r_1^2/r_2$ where r_2 = radius up to the location of the compression force resultant N_f in the fracture process zone [Fig. 8(a) and (b)]. We may assume that $r_2 = k_2 r_1$ where k_2 = empirical constant greater than 1 but close to 1. Approximately, we may write $\bar{\sigma}_1 = k_1 f_t'$, where k_1 = empirical constant of the order of 1, perhaps k_1 = 0.5 to 1.0, and f_t' = direct tensile strength of concrete. Solving for N_f, we get

$$N_f = -\frac{k_1 f_t'}{2k_2} r_1 \tag{6}$$

For the previous Mode II fracture tests of Bažant and Pfeiffer,[1] a similar equilibrium condition for the fracture-plane cross section yields tensioned portion of the ligament [Fig. 8(c) and (d)]. Setting again $\bar{\sigma}_1 = k_1 f_t'$ we get

$$N_f = -c_1 k_1 f_t' \tag{7}$$

Let us assume that function $\phi(N_f)$ can be approximated linearly, i.e., $\phi(N_f) = G_0^s - k_f N_f$, where G_0^s = shear fracture energy at zero confining stress and k_f = nondimensional constant. For $N_f = c_f f_t'$ the fracture energy should become approximately zero, and so we have

$$\phi(N_f) = k_f (c_f f_t' - N_f) \tag{8}$$

Using Eq. (6) and (7) in Eq. (8), we obtain

$$\frac{G_f^{II}}{G_f^{III}} = \frac{c_f + k_1 c_1}{c_f + r_1 K_1/2K_2} \tag{9}$$

Since the fracture energy is defined for the limit case of an infinitely large specimen, we must assume that $c_f \ll c_1$ and $c_f \ll r_1$; therefore

$$\frac{G_f^{II}}{G_f^{III}} = 2k_2 \frac{c_1}{r_1} \tag{10}$$

According to the results of the tests made (Table 2), $G_f^{II}/G_f^{III} \simeq 10$ for concrete and 3.3 for mortar. This ratio can be obtained from Eq. (10), given that $c_0 = r_0$, and if we assume intuitively that $k_2 = 1.5$, $c_1 = 0.7\, c_0$, and $r_1 = 0.21\, c_0$ for concrete; and $k_2 = 1.5$, $c_1 = 0.70\, c_0$, and $r_1 = 0.64\, c_0$ for mortar. These values do not appear to be out of the range of the reasonably expected behavior. So we may conclude that the difference between G_f^{II} and G_f^{III} is not all that surprising and might be explicable by a rational theory. But further tests as well as finite element studies will be required.

The previous analysis is based on the assumption of a linear dependence of G_f on N_f. In reality, this dependence must be expected to be nonlinear. Materials such as concrete exhibit a brittle-ductile transition at a certain confining pressure p_{bd}; for ordinary concrete, approximately, $p_{bd} \approx$ 10,000 psi (69 MPa). Above this pressure value, there is apparently no strain softening and no fracture, and so $G_f^s \to \infty$. To satisfy this condition, the nonlinear dependence of G_f on N_f may be assumed to have the form

$$G_f = \phi(N_f) = \alpha_1 (N_f - N_{bd})^{-n} + \alpha_2 \quad (N_f < N_{bd}) \tag{11}$$

where α_1, α_2, and n = empirical positive constants and $N_{bd} = c_f P_{bd}$. Constants α_1 and α_2 may be determined from two conditions: (1) $G_f^s = 0$ for $N_f = c_f f_t'$, and (2) $G_f^s = G_{f_0}^s$ for $N_f = 0$ where $G_{f_0}^s$ = shear fracture energy at zero normal force across the ligament. This yields

$$G_f^s = G_{f_0}^s \frac{(N_f - N_{bd})^{-n} - (N_0 - N_{bd})^{-n}}{(-N_{bd})^{-n} - (N_0 - N_{bd})^{-n}} \tag{12}$$

where $N_0 = c_f f_t'$. This nonlinear form of the function $\phi(N_f)$ can considerably alter the values in Eq. (10) which correspond to the observed ratio G_f^{III}/G_f^{II}.

The foregoing analysis has one weakness in that the size-effect law in Eq. (1), which underlies the determination of fracture energy, might not be valid when the value of the normal force N_f across the fracture-process zone is different for various sizes. If this were so, a more sophisticated extrapolation to infinite size would be required to obtain the fracture energy value. It remains to be seen whether this aspect can significantly affect the present results for the practical size range.

CONCLUSIONS

1. The size-effect method can be used to determine the shear fracture energy of concrete. A cylinder with a

circumferential notch, loaded in torsion, is a suitable test specimen and yields consistent results.

2. As expected according to the size-effect law, the test results for the mortar specimens are much closer to the linear-elastic fracture mechanics than the test results for the concrete specimens.

3. Although according to the elasticity theory, the notched cylindrical specimen yields a perfect shear state (characterized by antiplane symmetry of the stresses near the crack-front edge), it does not yield such a perfect state in practice because of nonlinear effects. These effects result from the transverse confining normal stresses which are produced in the ligament cross section due to volume expansion from microcracking in the fracture process zone.

4. The value of the fracture energy of concrete obtained from Mode III tests is about three times larger than the Mode I fracture energy and about ten times less than the Mode II fracture energy obtained with the double-notched four-point-loaded specimens used in previous tests.[1] For mortar, it is about eight times larger than the Mode I fracture energy and three and one-half times less than the Mode II fracture energy.

5. The discrepancies between the Mode II and Mode III shear-fracture energy values seem to be explained by inclined microcracking in the fracture-process zone, the associated volume change, and the induced compressive force across the fracture front. Because of the influence of this force, the shear fracture energy for Modes II and III (unlike the Mode I fracture energy) is not a material constant but must be considered to be a material function of the confining normal force.

6. The fact that the relative difference between the Mode III and Mode I fracture energies is less for mortar than for concrete indicates that the confining force across the fracture process zone [Eq. (6)] is apparently less for mortar than for concrete. This might be explained by a smaller volume expansion of mortar.

ACKNOWLEDGMENTS

Development of the underlying theory was supported under AFOSR contract No. F49620-87-C-0030DEF with Northwestern University. Partial support for the tests of mortar specimens was received under a cooperative research program with Universidad Politecnica de Madrid funded under a U.S.-Spain Treaty (grant CCA-8309071). Interpretation of the results was partially supported from the Center for Advanced Cement-Based Materials at Northwestern University (NSF grant DMR-880 8432).

REFERENCES

1. Bažant, Z. P., and Pfeiffer, P. A., "Shear Fracture Tests of Concrete," *Materials and Structures, Research and Testing* (RILEM, Paris), V. 19, No. 110, Mar.-Apr. 1986, pp. 111-121.

2. Ingraffea, A. R., and Panthaki, M. T., "Analysis of Shear Fracture Tests of Concrete," *Proceedings,* U.S.-Japan Seminar on Finite Element Analysis of Reinforced Concrete Structures (Tokyo, May 1985), American Society of Civil Engineers, New York, 1987, pp. 151-173.

3. Bažant, Z. P., and Pfeiffer, P. A., "Comment on Ingraffea and Panthaki's Analysis of Shear Fracture Tests of Concrete," *Proceedings,* U.S.-Japan Seminar on Finite Element Analysis of Reinforced Concrete Structures (Tokyo, May 1985), American Society of Civil Engineers, New York, 1987, pp. 174-183.

4. Bažant, Z. P., and Prat, P. C., "Measurement of Mode III Fracture Energy of Concrete," *Nuclear Engineering and Design* (Lausanne), V. 106, 1988, pp. 1-8. Also, *Report* No. 87-12/428m, Center for Concrete and Geomaterials, Northwestern University, Evanston, 1987.

5. Bažant, Zdeněk P., "Size Effect in Blunt Fracture: Concrete, Rock, Metal," *Journal of Engineering Mechanics,* ASCE, V. 110, No. 4, Apr. 1984, pp. 518-535.

6. Bažant, Zdeněk P., and Pfeiffer, Phillip A., "Determination of Fracture Energy from Size Effect and Brittleness Number," *ACI Materials Journal,* V. 84, No. 6, Nov.-Dec. 1987, pp. 463-480.

7. Bažant, Zdeněk P.; Kim, Jin-Keun; and Pfeiffer, Phillip A., "Nonlinear Fracture Properties from Size Effect Tests," *Journal of Structural Engineering,* ASCE, V. 112, No. 2, Feb. 1986, pp. 289-307.

8. Bažant, Z. P., and Kazemi, M., "Determination of Fracture Energy, Process Zone Length and Brittleness Number from Size Effect, with Application to Rock and Concrete," *Report* No. 88-7/498d, Center for Concrete and Geomaterials, Northwestern University, Evanston, May 1988, 36 pp. Also, *International Journal of Fracture,* in press.

9. Suresh, S., and Tschegg, E. K., "Combined Mode I - Mode III Fracture of Fatigue - Precracked Alumina," *Journal of the American Ceramic Society,* V. 70, No. 10, Oct. 1987, pp. 726-733.

10. Neville, A. M., *Properties of Concrete,* 3rd Edition, Pitman Publishing, Inc., Marshfield, 1981, 779 pp.

11. Bažant, Zdeněk P., "Fracture Mechanics and Strain-Softening of Concrete," *Proceedings,* U.S.-Japan Seminar on Finite Element Analysis of Reinforced Concrete Structures (Tokyo, May 1985), American Society of Civil Engineers, New York, 1987, pp. 121-150.

12. Bažant, Z. P., "Fracture Energy of Heterogeneous Material and Similitude," *Preprints,* SEM-RILEM International Conference on Fracture of Concrete and Rock (Houston, June 1987), Society for Experimental Mechanics, Bethel, pp. 229-241.

13. Bažant, Zdeněk P., and Kim, Jin-Keun, "Size Effect in Shear Failure of Longitudinally Reinforced Beams," ACI JOURNAL, *Proceedings* V. 81, No. 5, Sept.-Oct. 1984, pp. 456-468.

14. Bažant, Z. P.; Sener, S.; and Prat, P. C., "Size Effect Tests of Torsional Failure of Concrete Beams," *Report* No. 86-12/428s, Center for Concrete and Geomaterials, Northwestern University, Evanston, Dec. 1986, 18 pp. Also, *Materials and Structures, Research and Testing* (RILEM, Paris), V. 21, No. 126, Nov. 1988, pp. 425-430.

15. Bažant, Zdeněk P., and Cao, Zhiping, "Size Effect in Punching Shear Failure of Slabs," *ACI Structural Journal,* V. 84, No. 1, Jan.-Feb. 1987, pp. 44-53.

16. Bažant, Zdeněk P., and Cao, Zhiping, "Size Effect in Brittle Failure of Unreinforced Pipes," ACI JOURNAL, *Proceedings* V. 83, No. 3, May-June 1986, pp. 369-373.

17. Tada, H.; Paris, P. C.; and Irwin, G. R., *The Stress Analysis of Cracks Handbook,* Del Research Corp., Hellertown, 1973.

18. Benthem, J. P., and Koiter, W. T., "Asymptotic Approximation to Crack Problems," *Methods of Analysis of Crack Problems,* G. C. Sih, Editor, Noordhoff International Publishers, 1972, Chapter 3.

19. Bažant, Zdeněk P., and Oh, B. H., "Crack Band Theory for Fracture of Concrete," *Materials and Structures, Research and Testing* (RILEM, Paris), V. 16, No. 93, May-June 1983, pp. 155-177.